Image Features

Local Scale Control for Edge Detection and Blur Estimation

James H. Elder[1] and Steven W. Zucker[2]

[1] NEC Research Institute, Princeton, NJ, U.S.A.
[2] Centre for Intelligent Machines, McGill University, Montréal, Canada.

Abstract. Selecting the appropriate spatial scale for local edge analysis is a challenge for natural images, where blur scale and contrast may vary over a broad range. While previous methods for scale adaptation have required the global solution of a non-convex optimization problem [8], it is shown that knowledge of sensor properties and operator norms can be exploited to define a unique, locally-computable *minimum reliable scale* for local estimation. The resulting method for local scale control allows edges spanning a broad range of blur scales and contrasts to be reliably localized by a single system with no input parameters other than the second moment of the sensor noise. Local scale control further permits the reliable estimation of local blur scale in complex images where the conditions demanded by Fourier methods for blur estimation break down.

1 Introduction

Edge detectors are typically designed to recover step discontinuities in an image (e.g. [1–3, 11]), however the boundaries of physical structures in the world generally do not project to the image as step discontinuities, but as blurred transitions corrupted by noise (Fig. 1). This paper generalizes the detection of step discontinuities to encompass this broader, more physically realistic class of edges. We focus here on what can be computed from a *local* analysis of such luminance transitions.

Geometric models for focal and penumbral blur predict mathematically identical luminance transitions in the image, and shaded object edges can also mimic these patterns [4]. The goal of a local analysis must therefore be to reliably model luminance transitions over the broad range of conditions under which they occur, regardless of their physical origin.

To illustrate the challenge in achieving this goal, consider the scene shown in Fig. 2. Because the light source is not a point source, the contour of the cast shadow exhibits a broad variation in penumbral blur. On the left of Fig. 2 is shown the edge map generated by the Canny/Deriche edge detector [2,3], where the scale parameter has been tuned to detect the details of the mannequin. At this relatively small scale, the contour of the shadow cannot be reliably resolved and the smooth intensity gradients behind the mannequin are detected as many short, disjoint curves. On the right of Fig. 2 is shown the edge map generated by the Canny/Deriche edge detector tuned to detect the contour of the shadow. At

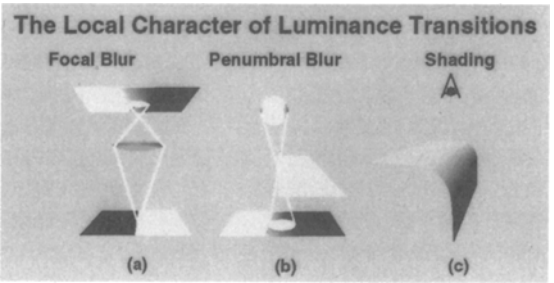

Fig. 1. Edges in the world generically project to the image as spatially blurred. From left to right: Focal blur due to finite depth-of-field; penumbral blur at the edge of a shadow; shading blur at a smoothed object edge.

this larger scale, the details of the mannequin are blurred out, and the contour of the shadow is fragmented at the section of high curvature under one arm.

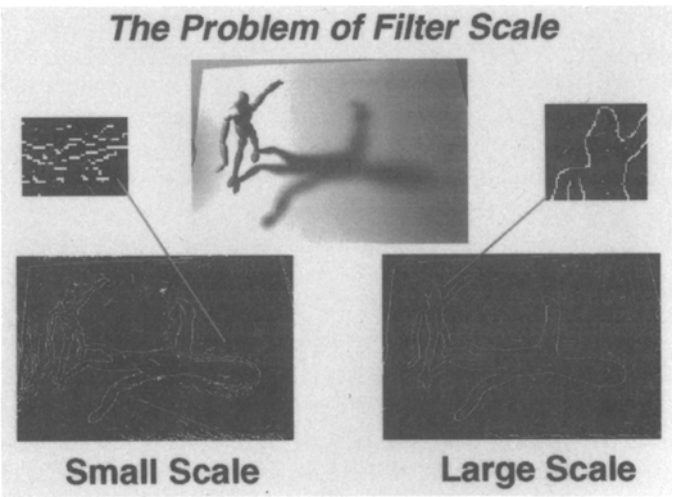

Fig. 2. Output of Canny/Deriche edge detector for small filter scale (left) and large filter scale (right).

This example suggests that to process natural images, operators of multiple scales must be employed. Of course, this conclusion has been reached by many computer vision researchers (e.g. [2,9,12,13,18]). However, the problem has been and continues to be: once a scale space has been computed, how is it used? Is

there any principled way to combine information over scale, or to reason within this scale space, to produce usable assertions about the image?

2 Minimum Reliable Scale

The difficulty in reliably recovering structure from images such as Fig. 2 is that the appropriate scale for estimation varies over the image. However, while the scale of the scene structure is space-variant, the properties of the sensor are typically fixed and known in advance. Given a specific model of a luminance edge, one can use knowledge of sensor noise properties to relate the parameters of the model to a unique minimum scale at which the edge can be reliably detected. We call this unique scale the *minimum reliable scale* for the edge.

By reliable here we mean that at this scale, the likelihood of error due to sensor noise is below a standard tolerance (e.g. 5% for an entire image). This definition does not account for the danger of incorrect assertions due to the influence of scene events nearby in the image, which in any band-limited system must be an increasing function of scale. While attempts have been made by others to explicitly model this phenomenon [2], it is our view that this problem is unlikely to admit such a general solution. For example, while an ensemble of images may yield an estimate of the expected separation between edges, if a sample of the ensemble contains a fine corduroy pattern, this estimate will be of little use. The method for local scale control developed here is based on the conjecture that, given no prior knowledge of the scene being imaged, the *most* reliable scale for local estimation is the *minimum* reliable scale, as defined above.

Jeong & Kim [8] have also proposed an adaptive method for estimating a unique scale for local edge detection. They pose the problem as the minimization of a functional over the entire image. They report that their results suffered from the complicated shape of the objective function, and the resulting sensitivity of the selected scale to the initial guess. It will be shown here that such problems can be avoided; that given an appropriate model for the sensor, estimation of the minimum reliable scale can be posed as a *local* problem.

3 Modelling Edges, Blur and Sensing

An edge is modeled as a step function $Au(x) + B$ of unknown amplitude A and pedestal offset B, which, for the purposes of this discussion, will be aligned with the y-axis of the image coordinate frame. The focal or penumbral blur of this edge is modelled by a Gaussian blur kernel, $g(x, y, \sigma_b) = \frac{1}{2\pi{\sigma_b}^2} e^{-(x^2+y^2)/2{\sigma_b}^2}$ of unknown scale constant σ_b. Sensor noise $n(x, y)$ is modeled as a stationary, additive, zero-mean white noise process with standard deviation σ_n. The complete edge model is thus:

$$(A/2)(erf(x/\sqrt{2}\sigma_b) + 1) + B + n(x, y) \tag{1}$$

An example of the model is shown in Fig. 3(a).

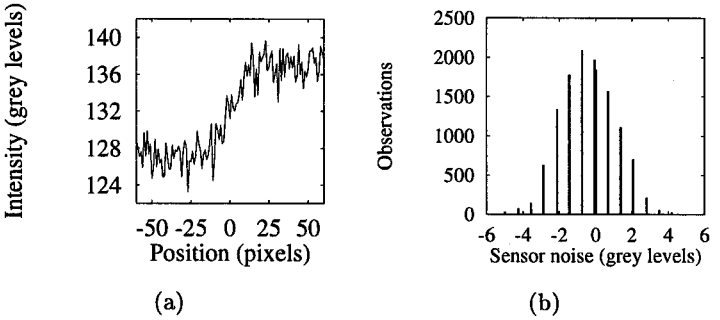

Fig. 3. a. The blurred edge model: $A = 10$ grey levels, $B = 127$ grey levels, $\sigma_b = 10$ pixels, $\sigma_n = 1.6$ grey levels. **b.** Histogram of estimated sensor noise

To estimate the sensor noise for the imaging system, a region of a defocused image of the ground plane shown in Fig. 2 was high-pass filtered with a unit-power kernel, the 2-tap filter $(1/\sqrt{2}, -1/\sqrt{2})$. The shading over this subimage varies slowly, and the defocus acts as an additional low-pass filter, so that the scene structure contributes negligible energy to the filter output. The following elementary result from the theory of random processes is now exploited [15]:

Proposition 1. *The standard deviation of a linear transformation $\mathcal{L} : \Re^n \to \Re$ of a set of i.i.d. random variables of standard deviation σ_n is the product of the L_2 norm of the linear transformation and the standard deviation of the random variables: $\sigma_{\mathcal{L}} = ||\mathcal{L}||_2 \sigma_n$.*

Thus the statistics of the unit-power filter output provide an estimate of the statistics of the sensor noise: a histogram is shown in Fig. 3(b). The standard deviation of the noise is approximately 1.6 quantization levels (for 8-bit images). The response of a unit-power operator is defined to be significant if it exceeds the mean response to white noise by $5\sigma_n$: 8 quantization levels in this case. Based on the normal model of sensor noise, the likelihood of an incorrect assertion for a single image of the size used here (256×384) is roughly 5%.

4 Local Scale Control and Gradient Estimation

A necessary condition for the local assertion of an edge is a non-zero gradient in the luminance function. The gradient can be estimated using steerable Gaussian first derivative basis filters [6,17]:

$$g_1^x(x,y,\sigma_1) = \frac{-x}{2\pi\sigma_1^4} e^{-(x^2+y^2)/2\sigma_1{}^2} \quad , \quad g_1^y(x,y,\sigma_1) = \frac{-y}{2\pi\sigma_1^4} e^{-(x^2+y^2)/2\sigma_1{}^2},$$

where σ_1 denotes the scale of the first derivative Gaussian estimator. The response $r_1^\theta(x,y,\sigma_1)$ of a first derivative Gaussian filter $g_1^\theta(x,y,\sigma_1)$ to an image $I(x,y)$ in an arbitrary direction θ can be computed exactly as a weighted sum of the basis filter responses:

$$r_1^\theta(x,y,\sigma_1) = \cos(\theta) r_1^x(x,y,\sigma_1) + \sin(\theta) r_1^y(x,y,\sigma_1).$$

At non-stationary points of the luminance function, $r_1^\theta(x,y,\sigma_1)$ has a unique maximum over θ, the gradient magnitude $r_1^{\theta_M}(x,y,\sigma_1)$, attained in the gradient direction $\theta_M(x,y,\sigma_1)$:

$$r_1^{\theta_M}(x,y,\sigma_1) = \sqrt{(r_1^x(x,y,\sigma_1))^2 + (r_1^y(x,y,\sigma_1))^2}$$
$$\theta_M(x,y,\sigma_1) = \arctan(r_1^y(x,y,\sigma_1)/r_1^x(x,y,\sigma_1))$$

For an image consisting of a blurred step edge along the y axis of amplitude A and blur parameter σ_b, the gradient magnitude attains its maximum on the y axis:

$$r_1^x(0,y,\sigma_1) = \frac{A}{\sqrt{2\pi(\sigma_b^2 + \sigma_1^2)}}. \tag{2}$$

To be confident that a non-zero gradient is due to the image and not to the noise, we must consider the likelihood that the response of the gradient operator could be due to noise alone. The second moment of the gradient operator can be expressed in terms of the second moments of the linear basis filter responses:

$$E[(r_1^{\theta_M}(x,y,\sigma_1))^2] = E[(r_1^x(x,y,\sigma_1))^2] + E[(r_1^y(x,y,\sigma_1))^2]$$

Using Proposition 1, we can write the second moment of the response of the gradient operator to the sensor noise alone as

$$\sqrt{E[(r_1^{\theta_M}(x,y,\sigma_1))^2]} = \sqrt{2}\sigma_n ||g_1^\theta(x,y,\sigma_1)||_2$$

Using the Cauchy inequality, this second moment can be used as a conservative estimate of the expected response of the gradient operator to the sensor noise, so that, using the chosen significance level of 5 standard deviations, it can be asserted that the gradient of the original image is non-zero if

$$r_1^{\theta_M}(x,y,\sigma_1) > 6\sqrt{E[(r_1^{\theta_M}(x,y,\sigma_1))^2]} = 6\sqrt{2}\sigma_n ||g_1^\theta(x,y,\sigma_1)||_2$$

The L_2 norm of the Gaussian first derivative operator at a point is given by $||g_1^\theta(x,y,\sigma_1)||_2 = 1/(2\sqrt{2\pi}\sigma_1^2)$ [4], thus we have the following

Definition 2. The *significance threshold function* $s_1(\sigma_1)$, tracing the threshold of reliability of the Gaussian gradient operator as a function of scale, is given by

$$s_1(\sigma_1) = 3\sigma_n/\sqrt{\pi}\sigma_1^2 \tag{3}$$

Combining Eqns. 2 and 3 and solving for σ_1, we derive the following

Proposition 3. *For a system with white sensor noise of standard deviation σ_n, and an edge of amplitude A and blur parameter σ_b, there exists a* **minimum reliable scale** $\hat{\sigma}_1$ *at which the luminance gradient can be reliably detected:*

$$\hat{\sigma}_1^2 = \frac{2}{c^2}(1 + \sqrt{1 + (c\sigma_b)^2}), \quad \text{where} \quad c = \sqrt{2}A/3\sigma_n.$$

In our experiments we attempt only to stay close to the minimum reliable scale by computing gradient estimates at octave intervals of scale, at each point using the smallest scale at which the gradient estimate exceeds the significance threshold function, i.e.

$$\hat{\sigma}_1(x, y) = \inf\{\sigma_1 : r_1^{\theta_M}(x, y, \sigma_1) > s_1(\sigma_1)\}$$

We tested this computation on the synthetic image of Fig. 4, a vertical edge blurred by a space-varying Gaussian kernel, corrupted by Gaussian i.i.d. noise. The minimum reliable scale space map for gradient estimation is shown in Fig. 4(b). Five scales were used: $\sigma_1 \in \{0.5, 1, 2, 4, 8\}$ pixels. Observe how the estimation scale increases as the strength of the gradient signal decreases.

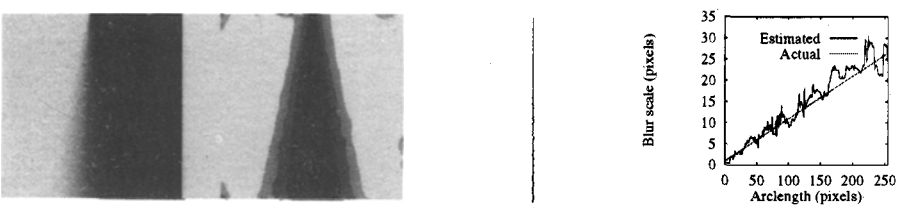

Fig. 4. Testing the local scale control algorithm on a synthetic image. **(a)** The blur grade is linear, ranging from $\sigma_b = 1$ pixel to $\sigma_b = 26.6$ pixels. Parameters (see Section 3): $A = B = 85$ grey levels, $\sigma_b \in [1, 26.6]$ pixels, $\sigma_n = 1.6$ grey levels. **(b)** Minimum reliable scale map for gradient estimation. Larger scales are rendered in lighter grey. White indicates that no reliable estimate could be made. **(c)** Detected edge. **(d)** Estimated blur scale.

The result of this gradient computation for the image of the mannequin and shadow is shown in Fig. 5(a). While the smallest scale is reliable for the contours of the mannequin, higher scales are required to fully recover the shadow. Note that significant gradients are also detected on the smoothly shaded ground surface: gradient information alone is clearly an insufficient basis for edge detection. We now proceed to develop the complete criteria for edge selection.

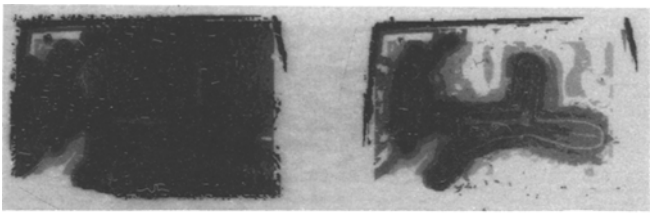

(a) (b)

Fig. 5. Maps of the minimum reliable scales for gradient and second derivative estimation, respectively. Larger scales are rendered in lighter grey.

5 Edge Detection and Localization

To distinguish edges from other forms of luminance gradients, we must somehow select for the sigmoidal shape that characterizes our edge model. This information is available in the second derivative of the luminance function, which can be estimated with a steerable second derivative of Gaussian operator, $g_2^\theta(x, y, \sigma_2)$ [4,6,17]. Since we are interested only in the luminance variation orthogonal to the edge, at each point in the image the second derivative is steered in the direction of the gradient estimated at the minimum reliable scale. As for the gradient, one can show that near an edge there exists a unique minimum scale at which the sign of the second derivative response $r_2^\theta(x, y, \sigma_2)$ can be reliably determined. A second derivative map is thus obtained which describes, at each point in the image where a significant gradient could be estimated, how this gradient is changing in the gradient direction (if at all). Six scales are employed to estimate the second derivative, at octave intervals: $\sigma_2 \in \{0.5, 1, 2, 4, 8, 16\}$ pixels. The minimum reliable scale map for the mannequin image is shown in Fig. 5(b).

The importance of the second derivative in localizing blurred edges is illustrated in Fig. 6. Fig. 6(b) shows the luminance profile through the edge of the mannequin's shadow. Fig. 6(d) shows the gradient magnitude along the cross-section, and Fig. 6(c) shows the minimum reliable scales at which the gradient was estimated. Note how the scale of estimation automatically adapts as the strength of the signal varies. Although this allows the gradient to be reliably detected as non-zero over this cross-section, the response is not unimodal: there are in fact 5 maxima in the gradient along the cross section of the edge. Marking edges at extrema in the gradient function would clearly lead to multiple separate responses to this single edge.

Fig. 6(f) shows the estimated second derivative steered in the gradient direction, and Fig. 6(e) shows the minimum reliable scales for these estimates. Note again how scale automatically adapts as the signal varies in strength: larger scales are needed near the centre of the edge where the luminance function is

nearly linear. Despite the rockiness of the gradient response, the adaptive second derivative response provides a unique zero-crossing to localize the edge, and strong extrema to identify its sigmoidal nature. The key here is that local estimation at the minimum reliable scale guarantees that the sign of the second derivative estimate is reliable, and hence that the zero-crossing is unique. The number of peaks in the gradient response, on the other hand, depends on the blur of the edge, and is not revealed in the response of the operator at any single point: ensuring the uniqueness of a gradient maximum is not a local problem. Thus the reliable detection and localization of blurred edges requires both gradient and second derivative information:

Definition 4. An **edge** exists at a point (x_0, y_0) if it satisfies 2 conditions:
Gradient Condition:
The gradient of the luminance function at the point is detectably non-zero:

$$\hat{\sigma}_1(x_0, y_0) = \inf\{\sigma_1 : r_1^{\theta_M}(x_0, y_0, \sigma_1) > s_1(\sigma_1)\} \neq \emptyset$$

Second Derivative Condition:
The second derivative of the luminance function in the gradient direction θ_M changes from positive to negative at the point:

$$r_2^{\theta_M}(x_+, y_+, \hat{\sigma}_2(x_+, y_+)) > 0 \quad , \quad r_2^{\theta_M}(x_-, y_-, \hat{\sigma}_2(x_-, y_-)) < 0$$

$$\begin{aligned} \textit{where} \quad x_- &= x_0 + \epsilon cos\theta_M \ , \quad y_- = y_0 + \epsilon sin\theta_M \\ x_+ &= x_0 - \epsilon cos\theta_M \ , \quad y_+ = y_0 - \epsilon sin\theta_M \end{aligned}$$

$$\begin{aligned} \textit{and} \quad \hat{\sigma}_2(x_+, y_+) &= \inf\{\sigma_2 : |r_2^{\theta_M}(x_+, y_+, \sigma_2)| > s_2(\sigma_2)\} \neq \emptyset \\ \hat{\sigma}_2(x_-, y_-) &= \inf\{\sigma_2 : |r_2^{\theta_M}(x_-, y_-, \sigma_2)| > s_2(\sigma_2)\} \neq \emptyset \end{aligned}$$

Here, ϵ is determined by the required localization precision: in this implementation, blurred edges are localized to 1 pixel precision. Note that, in general, $\hat{\sigma}_1(x, y) \neq \hat{\sigma}_2(x, y)$: the minimum reliable scales for estimating the gradient and second derivative are independent.

Roughly speaking, the above definition selects for points where the luminance function is detectably sigmoidal in shape. There is a strong connection between this definition and the machinery of logical/linear operators developed to detect in-focus edges [7].

Fig. 4(c) shows the edge points from the synthetic variable-blur image selected by Definition 4, using the local scale control algorithm. The edge is reliably and uniquely detected over a wide range of blur. Fig. 7 shows a map of the edge points in the image of the mannequin and shadow. Both the fine detail of the mannequin and the complete contour of the shadow are resolved, without spurious responses to the smooth shading gradients on the ground surface (compare with the results of the Canny/Deriche detector in Fig. 2.)

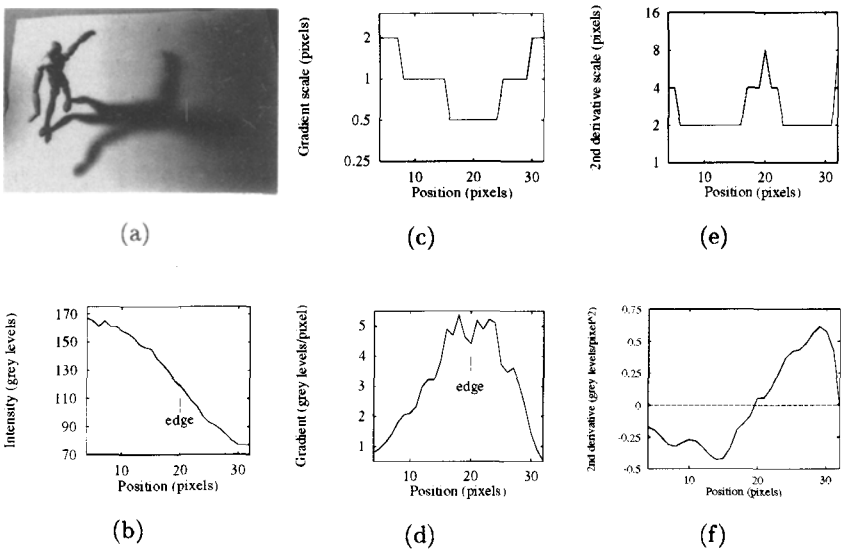

Fig. 6. **(a)** Mannequin shadow. White line indicates cross section of shadow boundary under analysis. **(b)** Cross section of luminance function across shadow boundary. **(c)** Minimum reliable scale for the gradient estimate. **(d)** Estimated gradient magnitude. **(e)** Minimum reliable scale for the second derivative estimate **(f)** Estimated directional second derivative. A unique zero-crossing localizes the edge.

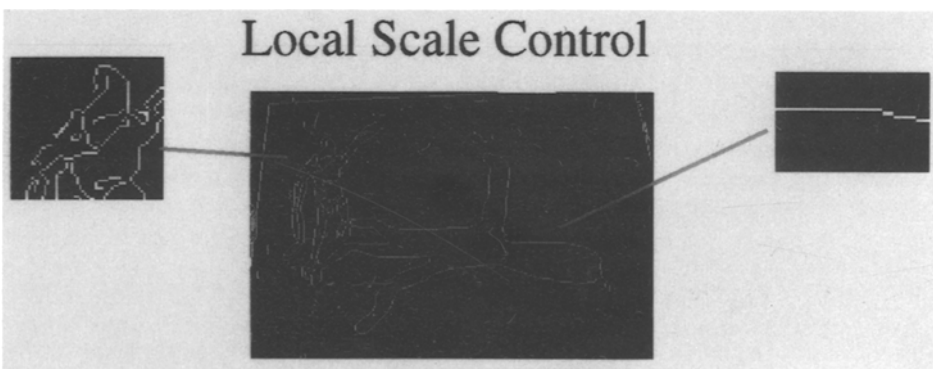

Fig. 7. Edges recovered from mannequin image using local scale control. Both the fine detail of the mannequin and the blurred boundary of the shadow are recovered.

6 Using Contour Blur to Estimate Defocus

Fig. 8(a) shows a tangle of branches, photographed with a shallow depth of field ($f/3.5$). Fig. 8(b) shows the edges detected for this image using local scale control for reliable estimation: both the in-focus and defocused branches are recovered.

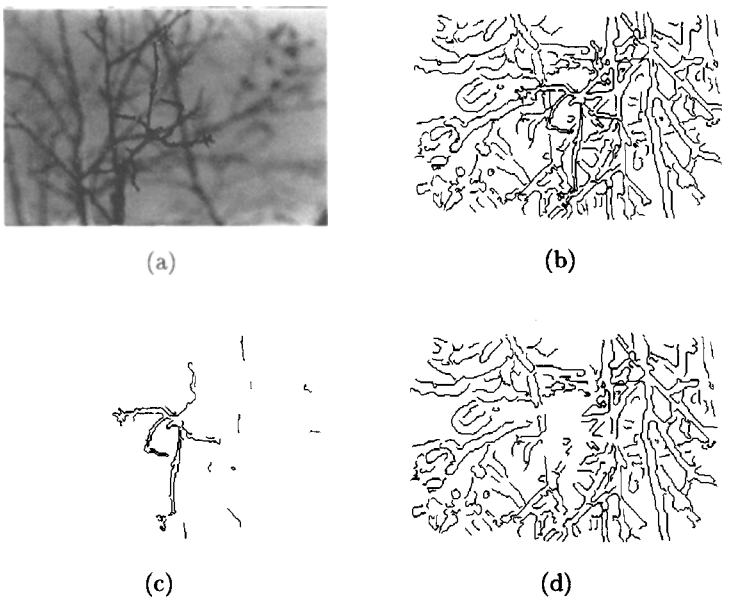

Fig. 8. **(a)** A photograph of tree branches with small depth of field ($f/3.5$) and near focus. **(b)** Edge map **(c)** Foreground structure (focused contours). **(d)** Background structure (blurred contours).

While excellent passive techniques for blur estimation have been developed, these typically require densely-textured surfaces varying slowly in depth [5, 14, 16] and are therefore not suited for recovering depth structure from a complex image such as this, where each local neighbourhood may contain many depth discontinuities. For such images, blur estimates can only be made where structure exists, and must be computed as locally as possible. The local scale control method can be extended naturally to this problem.

For the estimation of focal blur, the Gaussian kernel of our edge model represents the point spread function of the lens system of the camera employed. Without loss of generality, we again assume that the edge is oriented parallel to the y axis of the image plane. The extrema in the estimated second derivative occur at the zero-crossings x_M of the third derivative of the blurred step edge:

$$r_3^x(x_M, y_M, \sigma_2) = \frac{A}{\sqrt{2\pi(\sigma_2^2 + \sigma_b^2)}}((x_M^2/(\sigma_2^2 + \sigma_b^2) - 1)e^{-x_M^2/2(\sigma_2^2+\sigma_b^2)} = 0$$

so that $x_M = \pm\sqrt{\sigma_2^2 + \sigma_b^2}$. Defining d as the distance between second derivative extrema of opposite sign in the gradient direction, we obtain $\sigma_b = \sqrt{(d/2)^2 - \sigma_2^2}$. Thus the blur due to defocus can be estimated from the measured thickness of the contours, after compensation for the blur induced by the estimation itself.

Fig. 4(d) shows a plot of the estimated and actual blurs of the synthetic test image. While the resulting pointwise blur estimates are noisy, they provide an approximately unbiased estimate of the blur scale of the edge. This method for blur estimation was applied to the problem of segmenting the tangle of branches shown in Fig. 8. Fig. 8(c) and (d) show the extracted foreground (focused) and background (defocused) structure, respectively.

7 Space Curves from Defocus and Cast Shadows

While others have had some success in classifying contours as thin or diffuse [10, 19], this adaptive method for estimating contour blur can provide dense, accurate estimates *continuously* along image contours. As an example, consider the image of a model car (Fig. 9(a)) photographed with shallow depth of field ($f/2.5$). The lens was focused on the rear wheel of the car, so that the hood and front bumper are defocused. Fig. 9(b) shows the edges detected using local scale control. Fig. 9(c) shows a 3-D plot of one of the main contours of the car. Here the vertical axis represents the focal blur σ_b, estimated as described above, and smoothed along the contour with a Gaussian blur kernel ($\sigma = 22$ pixels). This adaptive method for blur estimation provides a continuous estimate of focal blur along the contour of the car.

This method for blur estimation can also be used to extract scene structure from penumbral blur (Fig. 9(d)). For a fixed light source, the penumbral blur is determined by the distance between the shadowing surface and the surface shadowed.[3] The results of penumbral blur estimation are shown in Fig. 9(e).

8 Conclusions

While edge detectors are typically designed to detect step discontinuities in images, physical edges in the world generally project to the image as blurred luminance transitions of unknown blur scale and contrast. In this paper, we have developed a method for adapting the spatial scale of local estimation to allow edges to be detected and characterized over this broad range of conditions.

[3] The estimation of distance from penumbral blur is more complicated than defocus, due to distortion caused by the slant of the ground surface relative to the observer and the light source. These estimates should therefore be viewed as qualitative.

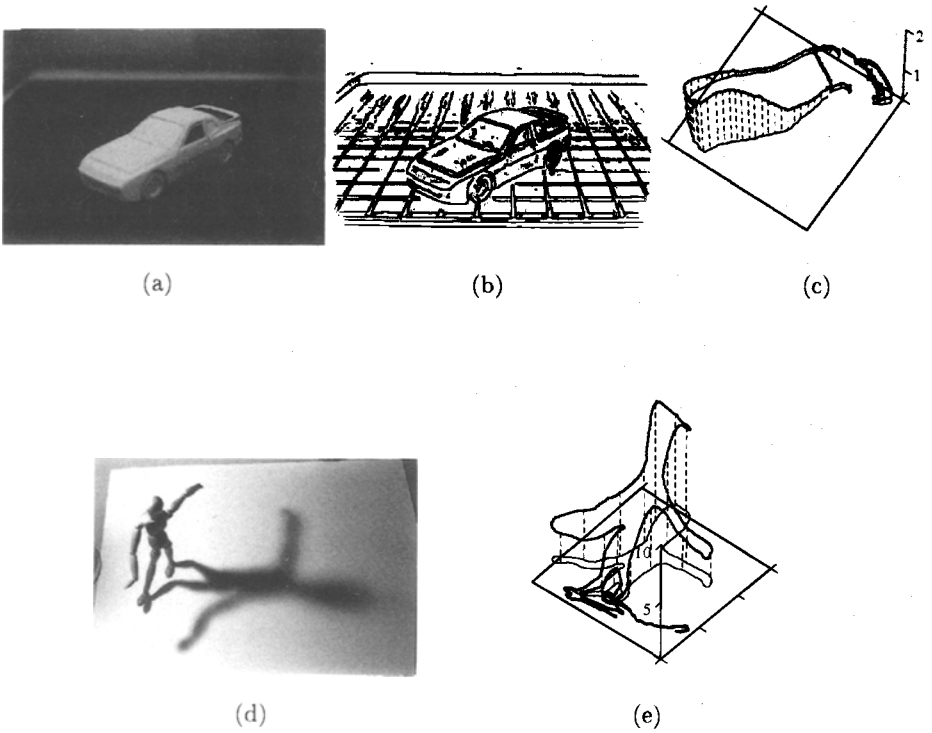

Fig. 9. **(a)** Photograph of car model with shallow depth of field ($f/2.5$). **(b)** Edges recovered using local scale control. **(c)** Space curve of contour from car. Estimated blur scale in pixels plotted on vertical axis. **(d)** Mannequin image with shadow. **(e)** Blur scale contour of mannequin shadow.

Specifically, this adaptive method reliably localizes edges while avoiding two important types of error: **(1)** multiple responses to a single transition, and **(2)** blurring of fine structure. This method for local scale control was further exploited to compute reliable estimates of local blur in complex images which do not satisfy the smoothness and texture density conditions required by traditional methods. These algorithms require no input parameters other than the second moment of the sensor noise.

References

1. A. Blake and A. Zisserman. *Visual Reconstruction.* MIT Press, Cambridge, Mass., 1987.
2. J.F. Canny. Finding edges and lines in images. Master's thesis, MIT Artificial Intelligence Laboratory, 1983.
3. R. Deriche. Using Canny's criteria to derive a recursively implemented optimal edge detector. *Int. J. Computer Vision*, 1(2):167–187, 1987.
4. J. Elder. *The visual computation of bounding contours.* PhD thesis, McGill University, Dept. of Electrical Engineering, 1995.
5. J. Ens and P. Lawrence. Investigation of methods for determining depth from focus. *IEEE Trans. Pattern Anal. Machine Intell.*, 15(2):97–108, 1993.
6. W.T. Freeman and E.H. Adelson. The design and use of steerable filters. *IEEE Trans. Pattern Anal. Machine Intell.*, 13(9):891–906, 1991.
7. L. Iverson and S.W. Zucker. Logical/linear operators for image curves. *IEEE Trans. Pattern Anal. Machine Intell.*, 17(10):982–996, 1995.
8. H. Jeong and C.I. Kim. Adaptive determination of filter scales for edge detection. *IEEE Trans. Pattern Anal. Machine Intell.*, 14(5):579–585, 1992.
9. J. Koenderink. The structure of images. *Biol. Cybern.*, 50:363–370, 1984.
10. A.F. Korn. Toward a symbolic representation of intensity changes in images. *IEEE Trans. Pattern Anal. Machine Intell.*, 10(5):610–625, 1988.
11. Y.G. Leclerc. The local structure of image discontinuities in one dimension. *IEEE Trans. Pattern Anal. Machine Intell.*, 9(3):341–355, 1987.
12. T. Lindeberg. Scale-space for discrete signals. *IEEE Trans. Pattern Anal. Machine Intell.*, 12(3):234–254, 1990.
13. D. Marr and E. Hildreth. Theory of edge detection. *Proc. R. Soc. Lond. B*, 207:187–217, 1980.
14. S.K. Nayar and N. Yasuo. Shape from focus. *IEEE Trans. Pattern Anal. Machine Intell.*, 16(8):824–831, 1994.
15. A. Papoulis. *Probability, Random Variables and Stochastic Processes.* McGraw-Hill, New York, 1965.
16. A.P. Pentland. A new sense for depth of field. *IEEE Trans. Pattern Anal. Machine Intell.*, 9(4):523–531, 1987.
17. P. Perona. Deformable kernels for early vision. *IEEE Trans. Pattern Anal. Machine Intell.*, 17(5):488–499, 1995.
18. A. Witkin. Scale space filtering. *Proc. Int. Joint Conf. on Artif. Intell.*, pages 1019–1021, 1983.
19. W. Zhang and F. Bergholm. An extension of Marr's signature based edge classification and other methods determining diffuseness and height of edges, and bar edge width. *Proc. 4^{th} Int. Conf. on Computer Vision*, pages 183–191, 1993.